

Dusty ERO Search behind Two Massive Clusters

Tadafumi TAKATA¹, Nobunari KASHIKAWA², Kouichiro NAKANISHI³,
 Kentaro AOKI¹, Ryo ASAI², Noboru EBIZUKA⁵, Motoko INATA⁴, Masanori IYE²,
 Koji S. KAWABATA², George KOSUGI¹, Youichi OHYAMA¹, Kiichi OKITA⁴,
 Toshiyuki SASAKI¹, Yoshihiko SAITO², Kazuhiro SEKIGUCHI¹, Yasuhiro SHIMIZU⁴,
 Hiroko TAGUCHI², and Michitoshi YOSHIDA⁴

¹*Subaru Telescope, National Astronomical Observatory of Japan,*

650 North A'ohoku Place, Hilo, Hawaii 96720, U.S.A.

takata@naoj.org

²*Opt/IR Astronomy Division, National Astronomical Observatory,*

2-21-1 Osawa, Mitaka, Tokyo 181-8588, Japan

³*Nobeyama Radio Observatory, National Astronomical Observatory,*

462-2 Nobeyama, Minamimaki, Minamisaku, Nagano 384-1305, Japan

⁴*Okayama Astrophysical Observatory, National Astronomical Observatory,*

Kamogata, Asakuchi, Okayama 719-0232, Japan

⁵*RIKEN(The Institute of Physical and Chemical Research),*

2-21 Hirosawa, Wako, Saitama 351-0198, Japan

(Received 2002 December 7; accepted 2003 June 10)

Abstract

We performed deep K' -band imaging observations of 2 massive clusters, MS 0451.6 – 0305 at $z = 0.55$ and MS 0440.5 + 0204 at $z = 0.19$, for searching counterparts of the faint sub-mm sources behind these clusters, which would provide one of the deepest extremely red object(ERO) samples. Comparing our near-infrared images with optical images taken by the Hubble Space Telescope and by the Subaru Telescope, we identified 13 EROs in these fields. The sky distributions of EROs are consistent with the previous results, that there is a sign of strong clustering among detected EROs. Also, the surface density with corrected lensing amplification factors in both clusters are in good agreement with that derived from previous surveys. We found 7 EROs and 3 additional very red objects in a small area (~ 0.6 arcmin 2) of the MS 0451.6 – 0305 field around an extended SCUBA source. Many of their optical and near-infrared colors are consistent with dusty star-forming galaxies at high redshifts($z \sim 1.0$ –4.0), and they may be constituting a cluster of dusty starburst galaxies and/or lensed star-forming galaxies at high redshift. Their red $J - K'$ colors and faint optical magnitudes suggest they are relatively old massive stellar systems with ages(>300 Mega years) suffering from dust obscuration. We also found a surface-

density enhancement of EROs around the SCUBA source in the MS 0440.5 + 0204 field.

Key words: galaxies: clusters: individual(MS 0451.6 – 0305, MS 0440.5 + 0204) — galaxies: evolution — galaxies: high-redshift — galaxies: individual(SMM J04542 – 0301, SMM J04541 – 0302)

1. Introduction

Following the commissioning of SCUBA on JCMT(Holland et al. 1999), sub-mm surveys of distant universe have rapidly increased the number of sub-mm selected galaxies (Hughes et al. 1998; Eales et al. 1999; Barger et al. 1998; Smail et al. 1997, 2002a; Chapman et al. 2002a; Fox et al. 2002; Scott et al. 2002). The advantages of selecting high-redshift objects based on a sub-mm wavelength are not only their negative k -correction up to $z \sim 10$ (Blain et al. 2002) but also their high sensitivity to very dusty objects, which are believed to be undergoing vigorous star formation at high redshift [their median redshift is revealed to be ~ 2.4 (Smail et al. 2002a; Chapman et al. 2003)]. They are one of the candidates of forming giant elliptical galaxies based on the current observational and theoretical predictions (Lilly et al. 1999). Although a very limited number of optical counterparts have been identified spectroscopically, they show notable diversity in their morphology (extended and/or merging), AGN possessions, dust temperatures, and so on (Smail et al. 2002a). To study the mechanisms of galaxy formations, such as merging and/or gravitational collapses, we need to clarify the nature and the environments of these faint sub-mm sources. Clearly, we need a much larger sample of faint sub-mm sources than we currently have. It also helps for comparing their features with nearby analogous objects, such as ultra-luminous IRAS galaxies and/or some other dusty populations detected by ISO, MAMBO, etc. These populations might be missed by the popular “Lyman Break galaxy surveys” [there are only few cases of Lyman Break galaxies with sub-mm detection (e.g. Chapman et al. 2002c)]. On the other hand, as firstly reported by Cimatti et al.(1998), there is some evidence that many of the sub-mm sources are associated with EROs(extremely red objects)(Cimatti et al. 1998; Blain et al. 2002; Smail et al. 2002a; Ivison et al. 2002; Wehner et al. 2002; Frayer et al. 2003). EROs have red colors, which is consistent with elliptical galaxies at high redshift, and they are separated into two categories of dusty starburst population and passively evolved stellar systems. The former are believed to be young high-redshift objects with a large star-formation rate, and their features are consistent with forming elliptical galaxies based on theoretical predictions. Therefore, searching for EROs associated with faint SCUBA sources is one of the most effective methods for detecting obscured (dusty) star-forming galaxy at high redshift, though it may be limited only for $z \leq 3$, because of large extinction of their optical(rest UV) light by their internal dust. There have been

several studies (Smail et al. 1999; Ivison et al. 2000; Frayer et al. 2000; Barger et al. 2000; Lutz et al. 2001; Frayer et al. 2003) which identified the ERO counterparts of the sub-mm sources. Furthermore, Ivison et al.(2000) succeeded to obtain the redshifts of SCUBA sources at $z \sim 2.56$ and $z \sim 2.2$ in the A 1835 region, and there are some lower redshift samples with spectroscopically determined redshifts(e.g. Smith et al. 2001). The lack of a suitable sample is partly because of their optical faintness. Thus, it is needed to search for ERO counterparts to those sub-mm sources that are optically bright enough for detailed spectroscopic studies.

Using the gravitational lensing effect as a natural telescope, which amplifies the brightness of distant objects behind the lens, is one of the most powerful methods for obtaining detailed information on intrinsically faint objects. There have been many successful results in observing various types of high redshift galaxies using this effect, such as Lyman break galaxies(Pettini et al. 2000; Franx et al. 1997), faint SCUBA sources(Ivison et al. 2000; Ivison et al. 2001; Ledlow et al. 2002) and EROs(G.P. Smith et al. 2002). The advantages of using the lensing effect is not only its photometric, but also spatial magnification, which will provide enlarged images of smaller distant objects, corresponding to a very high effective spatial resolution, which could not be achieved by the usual ground based observations. By using these effects, we could investigate the detailed structures and also the environmental status of distant objects.

In order to search for bright counterparts of SCUBA sources and to investigate their surrounding environments in detail, we performed ERO search observations behind 2 massive clusters of galaxies, MS 0451.6 – 0305 ($z = 0.55$) and MS 0440.5 + 0204 ($z = 0.19$). These clusters were discovered in the Einstein Medium Sensitivity Survey(EMSS)(Gioia et al. 1990), and were covered by a SCUBA mapping observation by Chapman et al.(2002a) and Smail et al.(1998; 2002a).

In the next section, we describe our data collection, including our observations. In section 3, we address the result of our imaging surveys and the various features of the candidates of the SCUBA source counterparts. A discussion is given in section 4. In this paper we use the cosmological parameters $H_0 = 60.0 \text{ km s}^{-1} \text{ Mpc}^{-1}$, $\Omega_M = 0.3$, and $\Omega_\Lambda = 0.7$. All magnitudes without any notice are given in Vega magnitude. We used the values in Fukugita et al. (1996) for converting between the AB and Vega scale magnitudes.

2. Observation, Data, and Data Reduction

2.1. Optical Data

2.1.1. HST data

Deep optical imaging data for both clusters taken by WFPC2 through a F702W filter were retrieved from the HST¹ archive system at STScI. The total exposure times for each cluster were 10400 seconds for MS 0451.6 – 0305 (Program ID 5987) and 22200 seconds for MS 0440.5 + 0204 (Program ID 5402), respectively. We used a post-calibrated data and combined them into one image by a drizzling technique implemented in ‘dither’ package in STSDAS, running in the IRAF² environment (Fruchter, Hook 2002). The depths for both images are 26.3 and 26.6 ST-mag(R_{ST})(assuming 2” diameter aperture with 2σ detection), respectively.

2.1.2. Optical imaging with Subaru Telescope

Optical imaging using Kron–Cousin’s R_c and I_c band filters for complementing WFPC2 data were performed for MS 0451.6 – 0305 using the Faint Object Camera and Spectrograph(FOCAS)(Kashikawa et al. 2002) at the Cassegrain focus of Subaru Telescope on 2000 December 29, during a commissioning observation run of FOCAS. Johnson B and SDSS z' imaging observations were performed on 2002 November 1 and 2, using Subaru Prime Focus Camera(SuprimeCam) (Miyazaki et al. 2002) attached to the prime focus of the Subaru telescope. All these images, except for z' -band image, were taken under good photometric conditions. The total exposure times were 3600, 1800, 1800 and 2940 s for the B , R_c , I_c and z' -bands, respectively. We applied the standard calibration for these data using IRAF tasks for the FOCAS data, and the software package for SuprimeCam data (Yagi et al. 2002). Photometric calibrations were performed using “RUBIN 152” in Landolt’s standard stars catalog (Landolt 1992) for the FOCAS data, and SA 95 for the SuprimeCam data (J.A. Smith et al. 2002). The limiting magnitudes of the images were 27.3, 25.6, 24.5, and 24.6 mag for the B , R_c , I_c and z' -bands, respectively, for 1σ detection within 2”diameter. Photometric errors for each band were estimated as being equal or less than 0.1 magnitude, except for the z' -band (~ 0.2). For a z' photometric calibration, we used images taken by HST/ACS through F850LP filter, and confirmed the accuracy of our photometry to be less than 0.2 magnitude. We used the STSDAS synphot package to convert from F850LP magnitude to z' magnitude. The seeing sizes were 0.6, 0.6, 0.55, and 0.7 arcsec for the B , R_c , I_c and z' band respectively.

We also retrieved Johnson V image taken by SuprimeCam with 3600 seconds exposure

¹ Based on observations made with the NASA/ESA Hubble Space Telescope, obtained from the data archive at the Space Telescope Science Institute. STScI is operated by the Association of Universities for Research in Astronomy, Inc. under NASA contract NAS 5-26555.

² IRAF is distributed by the National Optical Astronomy Observatories, which are operated by the Association of Universities for Research in Astronomy, Inc., under cooperative agreement with the National Science Foundation.

from SMOKA(Subaru Mitaka Okayama Kiso Archive system)³ (Baba et al. 2002), and reduced it in the standard manner. We performed a photometric calibration using standard stars in SA 95 and SA 107(Landolt 1992), and estimated the limiting magnitude (2" aperture with 1σ) to be 26.7. We checked the catalog with published V magnitude data of the same field (Stanford et al. 2002), and estimated the errors to be within 0.1 magnitude.

2.2. Near-Infrared Imaging

K' -band imaging observations were performed on 2000 November 17 and 18, and J -band imaging observation was made on 2002 January 6, using the Cooled Infrared Spectrograph and Camera for OHS(CISCO)(Motohara et al. 2002) attached to the Nasmyth focus of Subaru Telescope. Both clusters' images were taken by using 8 points dithering of 12 exposures with 20 s each for the K' -band and of 6 exposures with 40 s for the J -band, covering about a $2'.0 \times 2'.0$ field of view. The total exposure times were 9220 s in the K' -band, and 3600 s in the J -band for MS 0451.6 – 0305 and 6880 s in the K' -band for MS 0440.5 + 0204. The seeing sizes were $0''.6$ to $0''.8$ in the K' -band, and $0''.7$ to $0''.9$ in the J -band. The sky conditions were mostly photometric during the observation in 2000 November, but not on 2002 January 6. We used FS10 and FS12 from the UKIRT faint standard catalog (Casali & Hawarden 1992) for photometric calibrations. The depth of our observations reached to 22.1 mag in K' and 22.3 mag in J with 1σ detection within 2" diameter. For K' , we estimated the errors in our photometry to be less than 0.1 magnitude, but we could not confirm the error for the J -band using our data set, because it was not taken under photometric condition. Therefore, we compared the J -band magnitudes of our sample with those of a somewhat shallower sample by Stanford et al (2002) with a limiting magnitude of about 20.5, and found no systematic difference between these two datasets(less than 0.1 mag in r.m.s).

Astrometric calibrations were performed using USNO-A2.0 catalog in each field. For MS 0451.6 – 0305, we used the B -band SuprimeCam image for obtaining a wider field of view and about 900 stars with r magnitudes between 16 to 18 for fitting (for avoiding the position measurement error by saturation). After the fitting, we applied the measured positions of objects in the CISCO K' image and refit them. We used the HST F702W image for MS 0440.5 + 0204 with 10 stars, because it is the widest image for this field. The resultant r.m.s in the fittings were $0''.20$ and $0''.36$ for MS 0451.6 – 0305 and MS 0440.5 + 0204, respectively.

3. Results

3.1. Sample Extraction and Completeness

We used SExtractor (Bertin, Arnouts 1996) for making the K' -band selected catalog, which reached to a depth of ~ 22.1 magnitude in 2" diameter aperture. An eye inspection

³ <http://smoka.nao.ac.jp>.

was also carried out for all extracted sources, and spurious sources were eliminated from the sample. Photometry of other bands' images was carried out using the "double image mode", based on the K' -band image. For obtaining precise color information, we applied Gaussian smoothing to $B, V, F702W, R_c, I_c, z'$, and K' frames for matching the image qualities to that of the J -band, which had the worst seeing size. We set the detection criteria at 15 contiguous pixels ($0''.105 \text{ pix}^{-1}$) exceeding 1.5σ levels, and detected 235 and 164 objects with $K' \leq 22.0$ for MS 0451.6 – 0305 and MS 0440.5 + 0204, respectively. The following results and discussions are based on the magnitudes with $2''$ -diameter photometry, which corresponds to a linear scale of about 7 kpc and 15 kpc for $z = 0.19$ and 0.55, respectively.

The completeness of our catalog was estimated by adding artificial objects to the K' images for each field at empty positions. We used the IRAF package artdata for simulating and adding point-like sources as well as objects with de Vaucouleurs and exponential profiles (convolved with the seeing PSF) onto the images. SExtractor was run with the same detection parameters as for the real data. The limiting magnitudes with 80% completeness for each field were 21.5 for MS 0451.6 – 0305, and 21.7 for MS 0440.5 + 0204, respectively, using point sources, and they decreased to about 65% for objects with exponential profiles at these magnitudes. The completenesses at $K' = 22.0$ of point-source detection were $\sim 50\%$ and $\sim 60\%$, respectively for MS 0451.6 – 0305 and MS 0440.5 + 0204.

We adopted the photometric system from Holtzman et al. (1995) for deriving the R_c -band magnitudes from the HST F702W-band data, which are suitable for comparing the previous ERO surveys. We assumed the color of Sbc galaxies at a redshift of $z = 1 - 2$ ($V - R \sim 1.1$), which is the same manner of transformation adopted by G.P. Smith et al. (2002). The systematic uncertainty of this conversion is ≤ 0.1 , which arises from the likely presence of both more and less evolved galaxies than the adopted Sbc spectral type. We independently checked the observed FOCAS R_c -band magnitudes with these transformed magnitudes for the same objects, and confirmed the consistency with each other. In the following discussions, we use the R_c -band magnitudes which were transformed from the F702W magnitudes.

figure 1 shows a K' vs $R_c - K'$ diagram for the 2 fields with lines of $R_c - K' = 5.3$ and 6.0, which are our used ERO selection criteria. Most of the objects are concentrated around $R_c - K' \sim 3 - 4$, which is consistent with the color of early-type galaxies of cluster members at the corresponding redshifts and is also consistent with the results of shallower observations by Stanford et al. (1998) for MS 0451.6 – 0305.

There are 2(8) EROs in the MS 0451.6 – 0305 region with $R_c - K' \geq 6.0(5.3)$, and the number density is $0.5(2.0) \text{ arcmin}^{-2}$ down to $K' = 20.8$ [it is the limit of $R_c - K' > 5.3$ with $R_c < 26.1$ ($R_{\text{ST}} < 26.5$) sample], simply dividing the surveyed area (4 arcmin^2) without any correction for lens amplification. When limiting the magnitude with $K' = 20.0$, the numbers are reduced to 2(5). For MS 0440.5 + 0204, there are 0(5) EROs with $R_c - K' \geq 6.0(5.3)$, and the uncorrected number density is $0.0(1.25) \text{ arcmin}^{-2}$ down to $K' = 21.0$. When limiting the

magnitude with $K' = 20.0$, the numbers are reduced to 0(3).

figure 2 shows 3-color (R_c, I_c, K') image of MS 0451.6 – 0305 with $2' \times 2'$ field of view. There are some red objects which are bright in the K' band. figure 3 shows the sky distributions of EROs in MS 0451.6 – 0305 and MS 0440.5 + 0204, respectively for showing clustering properties in each field. It is clear that both in the MS 0451.6 – 0305 and the MS 0440.5 + 0204 regions, there is a non-uniform trend in the sky distribution of EROs and clustering in southern part of MS 0451.6 – 0305, while near the image center in MS 0440.5 + 0204.

3.2. Counterparts of SCUBA Sources

3.2.1. SCUBA sources in MS 0451.6 – 0305

Two sub-mm sources, SMM J 04542 – 0301 and SMM J 04541 – 0302, were detected in a survey of massive clusters using SCUBA by Chapman et al. (2002a).

SMM J 04542 – 0301 is located at $25''$ from the cluster center, and elongated to about $1'$ long, which is suggested to be a blend of multiple SCUBA sources (Chapman et al. 2002a). Its total flux at $850 \mu\text{m}$ is 19.1 mJy, and the magnification factor by cluster lensing is estimated to be 4.5. There is a constraint of the redshift for this source, as at $z \geq 2.3$ using the ‘sub-mm’ vs ‘cm’ spectral index (Yun, Carilli 2002). We found 7 EROs and 3 optically bright ($R_c \sim 23$ – 24) very red objects ($R_c - K' \sim 5$) around this sub-mm source, as shown in figure 4. The photometric parameters for these objects are summarized in table 1. “A1” and “A4” are very faint, even in a very deep (10400 s exposure) F702W image, and “A2” and “A3” are not visible in it. We plot $R_c - K'$ vs $J - K'$ diagrams to perform the diagnostics for distinguishing dusty star-forming EROs from passively evolved ones, as suggested by Pozzetti and Mannucci (2000) for identifying more plausible counterpart of the SCUBA source among those EROs in figure 5, in case they are at $1 < z < 2$. We also plotted the color tracks of elliptical and dusty starburst galaxies based on the GISSEL 99 model (Buruzal, Charlot 1993) for calculating the SEDs of each track. The ellipticals are represented by a simple stellar population with solar metallicity with Salpeter IMF with an age of 15 Gyrs. For dusty starbursts, we used a model with a constant star formation rate over 1Gyr reddened to $E(B - V) = 0.8$ using the dust-extinction law by Calzetti et al. (2000). We used the criteria suggested by Pozzetti and Mannucci (2000) for distinguishing two populations of EROs, which is $(J - K) = 0.34(R - K) + 0.19$ with $R_c - K' > 5.3$, and found that more than half of the EROs near the SCUBA source (“A1”, “A4”, “E” and “F”) can be categorized as dusty starburst populations. They may consist of groups of dusty EROs or some blends of lensed objects, because “A1” to “A4” are well aligned along another arc, which is denoted as “Blue Arc” in figure 4. It should be noted that if many of those EROs do not inhabit at $1.0 < z < 2.0$ this diagnostics are not very effective, because there will be overlaps of the occupation area between two classes of objects in color-color spaces. For higher redshift objects, it is suggested to use $J - K$ vs $H - K$ diagram in Pozzetti and Mannucci (2000). We could not perform this diagnostic because of a lack of H -band information for our sample. More

Table 1. Photometric properties of EROs and red objects around SMM J 04542 – 0301. The upper limits indicate the 3σ detection level in each band. The magnitudes are given in the Vega scale. All of them are observed magnitudes, and were not corrected for the lensing effect.

| Name | RA (J2000) DEC | | | Magnitudes(2''aperture) and colors | | | | | | | | |
|-----------------|----------------|-------------|-------|------------------------------------|-------------------|-------------------|-------|-------------------|------------|----------|------|--|
| | | K' | B | V | R_c | I_c | z' | J | $R_c - K'$ | $J - K'$ | | |
| A1 | 04:54:12.81 | –03:00:44.2 | 19.1 | 27.2 [†] | 26.3 [†] | 25.1 [†] | >24.5 | 24.4 [†] | >22.3 | 6.0 | >3.2 | |
| A2 | 04:54:12.82 | –03:00:47.6 | 20.1 | >27.3 | >26.7 | >26.0 | >24.5 | >24.6 | >22.3 | >5.9 | >2.2 | |
| A3 | 04:54:12.74 | –03:00:59.2 | 20.5 | 24.6* | 23.6* | >26.0 | >24.5 | 21.2* | >22.3 | >5.5 | >1.8 | |
| A4 | 04:54:12.68 | –03:01:01.3 | 19.0* | >27.3 | 26.3* | 25.4* | 24.4* | 23.7* | 22.1* | 6.4 | 3.1 | |
| A4(1'' ϕ) | | | 19.8* | >28.8 | 27.9* | 26.1* | 25.3* | 24.8* | 23.0* | 6.3 | 3.2 | |
| B | 04:54:13.43 | –03:00:42.9 | 19.4* | 27.3* | 25.5* | 24.5* | 23.6* | 23.2* | 22.0* | 5.1 | 2.6 | |
| B(1'' ϕ) | | | 20.1 | 28.4 | 26.7 | 24.8 | 24.4 | 24.1 | 23.1 | 4.7 | 3.0 | |
| C | 04:54:12.66 | –03:01:16.3 | 18.6* | 26.2* | 24.6* | 23.7* | 22.8* | 22.4* | 21.6* | 5.1 | 3.8 | |
| C(1'' ϕ) | | | 19.3 | 27.8 | 26.0 | 24.2 | 23.6 | 23.4 | 22.7 | 4.9 | 3.4 | |
| D | 04:54:12.33 | –03:01:15.6 | 19.4 | 27.0 | 25.9 | 24.4 | 24.1 | 23.6 | >22.3 | 5.0 | >2.9 | |
| E | 04:54:10.92 | –03:01:24.5 | 19.5 | 27.1 | 26.0 | 25.6 | >24.5 | >24.6 | >22.3 | 6.1 | >2.8 | |
| F | 04:54:11.22 | –03:01:22.9 | 19.7 | 26.8 | 26.6 | 25.5 | >24.5 | 23.8 | 22.1 | 5.8 | 2.4 | |
| G | 04:54:13.66 | –03:01:21.9 | 20.3 | >27.3 | >26.7 | >26.0 | >24.5 | >24.6 | >22.3 | >5.7 | 2.0 | |

† Possible another source.

* Possible contamination from other sources.

detailed discussions will be given in the next section.

SMM J 04541 – 0302 is unresolved in the SCUBA map at $65''$ from the cluster center, and lens amplification factor is 2.6 (Chapman et al. 2002a). The flux at $850\ \mu\text{m}$ is 16.8 mJy, and the constraint on photometric redshift derived from radio index is $z \geq 2.2$. Since this source is out of the field of view of our J and K' images, we can search for a counterpart only in optical B , V , R_c , I_c , and z' images taken by FOCAS and SuprimeCam. In these images, a relatively bright galaxy, with $R_c = 22.2$ with colors of $B - V = 1.3$, $B - R_c = 3.0$, $R_c - I_c = 1.0$ and $I_c - z' = 0.55$, is at nearly the SCUBA detection center. It has red colors, thus indicating a certain amount of dust obscuration. The SED fitting and photometric redshift estimate were carried out with hyperz (Bolzonella et al. 2000) with the information from these 5 bands. We had a fitting result with a dusty galaxy at low redshift (around $z \sim 0.6$) with $E(B - V) \sim 0.75$. It is a very possible counterpart for the sub-mm source, because it is believed to be suffering from large extinction by dust (figure 6). This galaxy is already listed in the catalog of the CNOC cluster survey (Ellingson et al. 1998), and its r and g magnitudes are 22.53 and 24.23, respectively, without information about the redshift. Since there is no information on near-infrared nor radio wavebands for the objects, it is very difficult to identify a secure counterpart.

The possibility of a sub-mm object lensed by a bright galaxy invisible in the optical bands, which was suggested by Chapman et al.(2002b), can not be eliminated.

3.2.2. *SMM J 04433 + 0210 in MS 0440.5 + 0204*

SMM J 04433+0210 was discovered in the “SCUBA Lens Survey” by Smail et al. (1997, 2002a), and its flux at 850 μ m is 7.2 mJy. There is no detected radio flux for this source down to the 70 μ Jy level at 1.4 GHz (Smail et al. 2002a). An optical counterpart was reported by Frayer et al. (2003) as “N4”, which was detected in their HST/F702W and K -band images. Their Keck spectroscopy revealed its redshift as being 2.51.

We measured the R_c magnitudes for this object as 25.4 and 26.1 for 2" and 1" apertures, respectively, although there is a certain amount of contamination from the neighboring bright galaxy “N1”, especially for a 2" aperture (figure 7). We also detected this object in the CISCO K' image (“B” in figure 7); the magnitudes are 19.5 and 20.3 for 2" and 1" apertures, respectively, which are in good agreement with the K magnitude in Smail et al. (1999) and Frayer et al. (2003). The estimated $R_c - K'$ color is 5.8 for 1" diameter magnitudes, and thus it is classified as EROs. It should be noted that there are two other EROs (“A” and “C”) within 10" of the sub-mm source.

4. Discussions

4.1. *Lens Model and Surface Density Calculation*

As shown in figure 3 and figure 4, there are concentrations of EROs within a small area in both fields. For discussing the surface-density enhancement, it is not straightforward to compare our sample with other wide-field ERO surveys, because our observation is targeted to the fields of cluster of galaxies. The effects by gravitational lensing, such as amplification of the source flux and the accompanying distortion of the background sky (source plane), should be taken into account. In such a case, lensing models can be used to compute the lens amplification as a function of the image plane position.

We modeled lensing clusters using an elliptical potential with the parameters listed in table 2. The lensing inversion was based on the prescription of Kormann et al. (1994) and Schneider et al. (1992), allowing calculations of the lensing amplification and distortion as a function of the position in the image plane. The essential parameters of the model are the redshift and the line-of-sight velocity dispersion of the cluster. The cluster ellipticity (f in table 2.) is chosen based on a measurement of each BCG (Brightest Cluster Galaxy) contour on the K' -band images.

The amplification imposed on each background galaxy depends on its redshift(z_{source}), and the redshift of the intervening lens (z_{lens}). We found that cumulative source counts depends weakly on the actual source redshift by investigating for the case of $z_{\text{source}} = 1.2, 1.5, 2.0, 2.5$, and 3.0, at which most of all EROs are expected to lie. Adopting a single value of z_{source}

introduced an uncertainty of at most less than 40% into the final surface density values for the whole field of view in MS 0451.6 – 0305, while it was less than 20% for MS 0440.5 + 0204. For overcoming these uncertainties, we adopted two single source planes of $z_{\text{source}} = 1.5$ and 3.0 , and used in each cluster model to compute a map of the lens amplification as a function of the image plane position for each value of z_{source} in each cluster field.

We first used the amplification maps to de-amplify the image plane flux of each EROs in our sample, and hence obtain their source plane K' -band magnitudes. Because gravitational lensing is achromatic, there is no need to correct the $R_c - K'$ colors. The number of EROs that are brighter than a source plane limiting magnitude can then be found by simply counting the number of sources brighter than the limiting magnitude in the source plane after correcting for lensing. A simple Poisson uncertainty is attached to this value.

We then calculated the area of the background sky within which EROs were detectable in the relevant cluster field in the following manner. An ERO with a source plane magnitude of K'_{source} will appear in the image plane of the relevant cluster with a magnitude brighter than an image plane detection limit of K'_{det} , if it is magnified by a factor greater than $\mu_{\text{min}} = 10^{-0.4(K'_{\text{det}} - K'_{\text{source}})}$. The area in the source plane within which such a galaxy would be detected in that cluster is thus $A(\mu_{\text{min}})$, where $A(\mu_{\text{min}})$ is the area of the $z_{\text{source}} = 1.5$ source plane behind each cluster that lies within the CISCO field of view, and is magnified by a factor greater than μ_{min} (figure 8). Therefore, we can derive the surface number density from the dividing number of galaxies by $A(\mu_{\text{min}})$.

4.2. Corrected Surface Density of EROs

The derived surface densities for each cluster field are 2.43 arcmin^{-2} for $R_c - K' \geq 5.3$ in MS 0451.6 – 0305, and 2.29 arcmin^{-2} for $R_c - K' \geq 5.3$ in MS 0440.5 + 0204 at $K' = 21.6$ for the source plane at $z_{\text{source}} = 1.5$. The cumulative surface densities as a function of the K'_{source} magnitude for a sample with $R_c - K' \geq 5.3$ are shown in figure 9. We also plotted the result for the 0.6 arcmin^2 area in MS 0451.6 – 0305 (rectangle surrounded by dotted lines in figure 3), in which 7 EROs were detected. About 20 and 10% of the whole survey areas reach to a depth of $K'_{\text{lim}} \sim 23.0$, when we adopt the detection limit as $K' = 22.0$. Because of the limit by the depth of the R -band magnitudes, the depth of our “ERO samples” are decreased to $K_{\text{source}} \sim 22.0$. Our sample thus provides one of the deepest ERO sample ever reported. It is noted that we obtained mostly the same results using other model parameters used in Wu et al. (1998) and Williams et al. (1999).

For a comparison, we overplotted the result of G.P. Smith et al.(2002) and Wehner et al.(2002) without the sample of A 2390 in figure 9. Both ERO samples were made by targeting lensing cluster fields, and selected by the same color criterion as ours ($R_c - K' > 5.3$). We also overplotted the results by blank-field ERO searches performed by Daddi et al.(2000), Roche et al.(2002), and Moustakas et al.(1997). G.P. Smith et al. (2002) surveyed lensed EROs

behind 10 massive clusters of galaxies around $z \sim 0.2$ to a depth of $K \sim 20.6$, and measured the surface density of 1.2 arcmin^{-2} for $R_c - K \geq 5.3$. They corrected the amplification effect from gravitational lensing using their own lens model, and estimated the corrected surface densities at $K \leq 21.6$ as 2.5 arcmin^{-2} . The values are very similar to our result. As shown in figure 9, there is little difference between both samples at the overlapping magnitude ranges, and can be considered to be within error bars for $R_c - K' \geq 5.3$ samples.

For a surface-density enhancement evaluation, we also calculated corrected surface densities in the areas which are shown in figure 3 by rectangles with dotted lines. In MS 0451.6 – 0305 field, 6 EROs in $\sim 0.6 \text{ arcmin}^2$ area, and the corrected surface density is 46.2 arcmin^{-2} down to $K'_{\text{source}} = 21.0$ at $z_{\text{source}} = 3.0$, or 30.8 at $z_{\text{source}} = 1.5$. In MS 0440.5 + 0204 field, 3 EROs brighter than $K' = 20.6$ are within 0.1 arcmin^2 area, and corrected surface density is 62.5 arcmin^{-2} down to $K'_{\text{source}} = 21.0$ at $z_{\text{source}} = 1.5$. They are more than 7-times than the average values reported by previous surveys. It is the same trend with the sample of G.P. Smith et al. (2002), which indicates that the numbers and sky distributions of EROs are very different in each field of view. Those are also consistent with the results by other wide field ERO surveys, which suggest the clustering properties of EROs (Daddi et al. 2001; Thompson et al. 1999). The most different property of our sample from G.P. Smith et al. (2002)'s is that most EROs identified in MS 0451.6 – 0305 show the colors which are common in dusty star-forming galaxies at high redshift (Figure 7), which indicate their strong star-formation activities, while most EROs are passively evolved objects in Smith et al.'s. Daddi et al. (2002) suggested that the strength of clustering is stronger in the old ERO population than that of dusty starburst EROs, and our results on the MS 0451.6 – 0305 may be a very rare case. It may indicate that the deeper is the depth of observation, for example down to $K' = 20.5$, the more will the ratio of dusty starbursts in ERO population increase. This is suggested by Smail et al. (2002b) with a radio-selected ERO sample, and the ratio of the dusty population to the passive one is comparable at brighter magnitudes (Cimatti et al. 2002). However, we also have to pay attention to the effect of the selection bias in our sample, which is made by targeting to lensed SCUBA sources, because it may increase the possibility of detecting dusty EROs.

In the deepest magnitude ranges of our sample, there are deficiencies of EROs compared to Wehner et al. (2002), while the uncertainties of ours and of their results are very large. This is because both surveys have a very limited region coverages and also suffer from field variances of ERO numbers.

4.3. Lensed Dusty Star-Forming Galaxies around SMM J 04542 – 0301?

4.3.1. Possible giant extremely red arc

As mentioned in the previous section, 7 EROs are concentrated within a 0.6 arcmin^2 sky area, and its corrected surface density is more than 7-times the average value (figure 9). For confirming the over density, however we have to take care of the fact that there are EROs

which are possible to be gravitationally lensed and separated (splitted) into several images (e.g. “A1” to “A4” in figure 4). These sources are well aligned in parallel to the “Blue Arc”, which is believed to be gravitationally elongated and split. If they are constructing an extremely red arc, the surface density will be decreased to 7.7 arcmin^{-2} for $z_{\text{source}} = 1.5$ or 23.1 arcmin^{-2} for $z_{\text{source}} = 3.0$ at $K'_{\text{source}} < 21.0$; however it is still a density enhancement.

For discussing the possibility of this lensing effect, we used the elliptical lens model, which was applied to a surface number count. The lens model also gives us a possibility to estimate the redshifts of lensed objects without any spectroscopic data, and may be able to set constraints on the spatial distribution of some EROs. We compared the critical curves on the image plane for different source plane redshifts, as shown in figure 10. We also overplotted the contour map of soft X-ray(0.2–1.5 keV) image of Chandra observation⁴ with 15000 s exposure⁵ to show the adequacy of our lensing model for approximating the cluster mass distribution. The images were retrieved from the Chandra archive, and we used CIAO software for extracting the soft band photon, combining each exposure and smoothing the resultant image. We applied 5-pixel Gaussian adaptive smoothing for the image using the csmooth task. The shapes of the inner X-ray contours and the used mass distribution are in good agreement for a first-order approximation of the mass distribution.

The sources “A1” to “A4” are very near to the critical curve, especially for $z_{\text{source}} = 1.2$ in figure 10. Therefore, it is possible that they are forming a large extremely red arc, and are split images of an object at $z \sim 1.2$. If they are, their colors must be very similar to each other, assuming no extinction differences along each light path. The colors of “A1” and “A4” are different, although the optical band magnitudes may be contaminated by other sources which are near to these objects. There remains a possibility that the colors of “A2” and/or “A3” will coincide with those of “A1” and/or “A4” because “A2” and “A3” are detected only in the K' band, and a color comparison was unavailable. Although the estimated redshifts is $z = 1.2$ by our lensing model, this is inconsistent with a photometric redshift of $z > 2.3$ derived from the radio vs sub-mm index if they are counterparts of the sub-mm source. However it is possible that the photometric redshift estimate is not appropriate if the assumed dust temperature for the SED model is not correct (Blain et al. 2003). In fact, it is suggested that there is a diversity of the dust temperature of sub-mm sources based on a sample of sub-mm sources with redshifts (Chapman et al. 2003).

It should also be noted that X-ray emission can not be completely fitted by a simple elliptical mass distribution. It is elongated to north-west direction, which has already been

⁴ Based in part on data retrieved from the Chandra Data Archive(CDA), a part of the Chandra X-ray Observatory Science Center(CXC) which is operated for NASA by the Smithsonian Astrophysical Observatory.

⁵ Because of spurious counts on a soft band image, we did not use the deeper (45000 s exposure) ACIS-S image for our analysis. For hard band image analysis, we used it.

suggested by Donahue et al. (1995) using the ROSAT image, and the X-ray contours are uneven(figure 10). For a more detailed discussion concerning the reality of a giant extremely red arc, it is necessary to use a lens model which is more sensitive to the local mass distribution, like that by Kneib et al.(1996). It will be considered in a future coming paper with some redshifts of bright objects and blue arcs.

4.3.2. SED fitting for a redshift estimation

For investigating the spatial clustering properties of these EROs and red galaxies near SMM J 04542 – 0301, we used a SED fitting for deriving the photometric redshifts for 6 objects among those (extremely) red objects (“A4”, “B”, “C”, “D”, “E”, and “F”), which had confirmed magnitudes in several bands. Because the optical bands’ lights of “A1” may be coming from a physically different source (optical centroids are more than 1” apart from K' image’s centroid), we eliminated “A1” from a list of our SED fitting. To avoid the effect of contamination from other surrounding sources, we used 1”diameter magnitudes for sources “A4”, “B”, and “C”, while they were 2”for others. We used hyperz for the calculation, by stepping the extinction from $A_V = 0.0$ to 5.0 using the extinction formula by Calzetti et al.(2000), and seeked the best solution in the range of $0.0 \leq z \leq 10.0$. As shown in figure 11, many objects, except for “D” and “F”, were fitted by SEDs of galaxies at high redshift($z \geq 2.6$), which are consistent with the photometric redshift from sub-mm to radio index($z_{\text{photo}} \geq 2.3$), although with relatively small extinction[$E(B - V) \sim 0.15 - -0.30$]. These extinction values are equal to, or slightly higher than, the median of those of Lyman break galaxies at $z \sim 3$ (Steidel et al. 1999; Shapley et al. 2001). Their $R - K'$ colors are more than 5.0, and thus redder than the sub-mm source Lyman break galaxy “W-MMD11” (Chapman et al. 2002c). They also have red $J - K'$ colors (> 2.3), and their properties are similar to those of a red massive galaxy population at high redshift($2 < z < 4$), revealed by the Faint InfraRed Extragalactic Survey(FIRE; Franx et al. 2003; van Dokkum et al. 2003). This red color can only be explained by a composite of the stellar ages with ≥ 300 Myr and a certain amount of obscuration by dust (Franx et al. 2003). The ages for our red sources best fitted by our analysis range from 0.5 to 1.2 Gyr. Daddi et al. (2003) suggested that their strong clustering at $2 < z < 4$ and our result can show the property. The derived extinction for “D” is large (0.89), and it is a plausible nearby candidate of a sub-mm source. Since the magnitudes of “A4” may be contaminated by neighboring foreground objects and/or contribution from diffuse emission by the cluster, the fluxes in the optical bands may be mainly coming from other sources. Therefore, it can have redder colors than those listed in table 1, and we could not eliminate the possibility of “A4” as being a counterpart of a sub-mm source. If so, its redshift can be higher, and may be the same as those of “B” and “C”. If “A1” to “A4” are constructing an extremely red arc, it is another plausible candidate of a sub-mm source, and they may have a spatial concentration with “B” and “C”.

It is noted that the results of photometric redshifts using different extinction models,

Table 2. Parameters of clusters used in the lensing model.

| Name | RA(J2000.0) | DEC(J2000.0) | z | $\sigma_{\text{los}}(\text{km s}^{-1})$ | Reference | f |
|------------------|-------------|--------------|------|---|------------------------|------|
| MS 0451.6 – 0305 | 04:54:10.8 | –03:00:51.6 | 0.55 | 1354 | Ellingson et al.(1998) | 0.9 |
| MS 0440.5 + 0204 | 04:43:09.9 | +02:10:19.8 | 0.19 | 872 | Gioia et al. (1998) | 0.95 |

like Fitzpatrick(1986) for Large the Magellanic Cloud or Prevot et al. (1984) and Bouchet et al. (1985) for the Small Megellanic Cloud, provided slightly higher redshifts.

By combining the result of our analysis, we can suggest one possibility that this extended sub-mm flux is coming from a high-redshift object, which must be lensed by a foreground cluster, and there may be a contribution from a lower redshifted ($z \sim 0.5$) dusty object, “D”. Since there is some evidence that Lyman break galaxies are not main contributor to the cosmic sub-mm background radiation (Adelberger, Steidel 1999; Webb et al. 2002), “B”, “C”, and “E” may be eliminated from the counterpart candidates; however, they may be spatially clustering near to the sub-mm emission. For secure counterpart identification and confirming the speculation of their clustering properties, it is essential to perform a deep radio interferometric observation and spectroscopic follow-up observations in optical or near-infrared wavelength.

Using Chandra hard (4–8keV) X-ray images, which was produced from the same data as that for figure 10, we checked the coincidences of X-ray detections around sub-mm sources in the MS 0451.6 – 0305 region, although no counterparts were identified. This is consistent with the result of previous studies because about 50000-s exposure by Chandra is not sufficient for detecting the X-ray flux from a large amount of sub-mm sources (Alexander et al. 2003; Waskett et al. 2003).

5. Summary

We performed deep near-infrared and optical imaging of two massive clusters of galaxy fields. By combining this data with photometric information taken from the deep WFPC2/F702W image, we identified EROs in each field, 8 in MS 0451.6 – 0305 and 5 in MS 0440.5 + 0204 with $R_c - K' \geq 5.3$, and $K' < 22.0$, in a $2' \times 2'$ field of view. Our sample provide one of the deepest sample of EROs ever reported. The surface density of our whole-area sample shows good agreement with other previous samples at the bright part. At the faint end, the number of EROs is slightly deficient compared to the previous work, though it is within the error bars.

We identified 7 EROs ($R_c - K' \geq 5.3$) and 3 red objects ($I_c - K' > 4.0$) with $K' \leq 20.6$ within 0.6 arcmin^2 of an extended SCUBA source in the MS 0451.6 – 0305 field. Our investigation using a lens model provided a value of surface density of EROs of $\sim 46 \text{ arcmin}^{-2}$ for $K'_{\text{source}} < 21.0$, showing a surface-density enhancement of extremely red galaxies, even after a correction of the lensing effect. It is possible that 4 sources, named “A1” to “A4”, constitute an

extremely red-giant arc, and that the best-fit redshift by our model is $z \sim 1.2$. The photometric redshift for a sub-mm source, derived based on the sub-mm to radio index, does not give consistent redshift. We also investigated the optical and near-infrared photometric features for the 6 red sources, and identified that 4 of them have SEDs which are typical of high-redshift objects. Their extinctions are typical, or slightly higher, values compared to those of Lyman break galaxies at $z \sim 3$. Our redshift estimation for “A4” based on an SED fitting is consistent with that from sub-mm to radio index, and it is possible to consider that “A1” to “A4” are lensed extremely red sources at $z > 2.5$, and a counterpart of an extended sub-mm source. One source with severe extinction is identified at a lower redshift ($z \sim 0.5$), and is one of the candidates of contributors to the extended sub-mm flux. For revealing their clustering properties and the relation with extended sub-mm emission, a spectroscopic follow-up observation in the optical and/or near-infrared wavelength is essential.

This study is based mainly on data collected at Subaru Telescope, and that obtained from the data archive at the Astronomical Data Analysis Center, which is operated by the National Astronomical Observatory of Japan. The authors thank an anonymous referee for valuable comments and suggestions for improving the manuscript. We are grateful to all Subaru staff members for their enormous help during our observations. T.T. thanks to Dr. Kentaro Motohara and Dr. Chris Simpson for their enormous help during the observation and data reduction, Dr. Yoshitomo Maeda for giving instructions on the CIAO software for reducing the Chandra image. T.T. also thanks the staff of the archive system of the Space Telescope Science Institute for their help in retrieving the HST data. This work is partly supported by the Ministry of Education, Culture, Sports, Science and Technology in Japan under Grant No. 12740126. K.N. has been financially supported by a JSPS Fellowship.

References

Adelberger, K.L., & Steidel, C.C. 2000, ApJ, 544, 218
 Alexander, D.M., et al. 2003 AJ, 125, 383
 Baba, H. et al. 2002, Rep. Natl. Astron. Obs. Japan, 6, 23 (in Japanese)
 Barger, A.J., Cowie, L.L., Sanders, D.B., Fulton, E., Taniguchi, Y., Sato, Y., Kawara, K., & Okuda, H. 1998, Nature, 394, 248
 Barger, A.J., Cowie, L.L., & Richards, E.A. 2000, AJ, 119, 2092
 Bertin, E., & Arnouts, S. 1998, A&AS, 117, 393
 Blain, A. W., Smail, I., Ivison, R.J., Kneib, J.-P., & Frayer, D.T. 2002, Physics Report, 369, 111
 Blain, A.W., Barnard, V.E. & Chapman, S.C. 2003, MNRAS, 338, 733
 Bolzonella, M, Miralles, J-M, & Pelló, R. 2000, A&A 363, 476
 Bouchet, P., Lequeux, J., Maurice, E., Prevot, L., & Prevot-Burnichon, M.L. 1985, A&A, 149, 330
 Bruzual, G.A., & Charlot, S. 1993, ApJ, 405, 538

Calzetti, D., Armus, L., Bohlin, R.C., Kinney, A.L., Koornneef, J., & Storchi-Bergmann, T. 2000, *ApJ*, 533, 682

Casali, M., & Hawarden, T. 1992, UKIRT Newsletter, 4, 33

Chapman, S.C., Scott, D., Borys, S.C., & Fahlman, G.G. 2002a, *MNRAS*, 330, 92

Chapman, S.C., Smail, I., Ivison, R.J., & Blain, A.W. 2002b, *MNRAS*, 335, 17

Chapman, S.C., Shapley, A., Steidel, C.C., & Windhorst, R. 2002c, *ApJ*, 572, L1

Chapman, S.C., Blain, A.W., Ivison, R.J., & Smail, I. 2003, *Nature*, 422, 695

Cimatti, A., Andreani, P., Röttgering, H., & Tilanus, R. 1998, *Nature*, 392, 895

Cimatti, A., et al. 2002, *A&A*, 381, L68

Daddi, E., Cimatti, A., Pozzetti, L., Hoekstra, H., Röttgering, H.J.A., Renzini, A., Zamorani, G., & Mannucci, F. 2000, *A&A*, 361, 535

Daddi, E., Broadhurst, T., Zamorani, G., Cimatti, A., Röttgering, H., & Renzini, A. 2001, *A&A*, 376, 825

Daddi, E., et al. 2002, *A&A*, 384, L1

Daddi, E., et al. 2003, *ApJ*, 588, 50

Donahue, M., & Stocke, J.T. 1995, *ApJ*, 449, 554

Eales, S. et al. 1999, *ApJ*, 515, 518

Ellingson, E., Yee, H.K.C., Abraham, R.G., Morris, S.L., & Carlberg, R.G. 1998, *ApJS*, 116, 247

Fitzpatrick, E. L. 1986, *AJ*, 92, 1068

Fox, M.J., et al. 2002, *MNRAS*, 331, 839

Franx, M., Illingworth, G.D., Kelson, D.D., van Dokkum, P.G., & Tran, K.-V. 1997, *ApJ*, 486, L75

Franx, M., et al. 2003, *ApJ*, 587, L79

Frayer, D.T., Smail, I., Ivison, R.J., & Scoville, N.Z. 2000, *AJ*, 120, 1668

Frayer, D.T., Armus, L., Scoville, N.Z., Blain, A.W., Reddy, N.A., Ivison, R.J., & Smail, I. 2003, *AJ*, in press(astro-ph/0304043)

Fruchter, A. S., & Hook, R. N. 2002, *PASP*, 114, 144

Fukugita, M., Ichikawa, T., Gunn, J.E., Doi, M., Shimasaku, K. & Schneider, D.P. 1996, *AJ*, 111, 1748

Gioia, I.M., Maccacaro, T., Schild, R.E., Wolter, A., Stocke, J.T., Morris, S.L., & Henry, J.P. 1990, *ApJS*, 72, 567

Gioia, I.M., Shaya, E.J., Le Févre, O., Falco, E.E., Luppino, G.A., Hammer, F. 1998, *ApJ* 497 573

Holland, W.S., et al. 1999, *MNRAS*, 303, 659

Holtzman, J.A., Burrows, C.J., Casertano, S., Hester, J.J., Trauger, J.T., Watson, A.M., & Worthey, G. 1995, *PASP*, 107, 1065

Hughes, D.H. et al. 1998, *Nature*, 394, 241

Ivison, R.J., Smail, I., Barger, A.J., Kneib, J.-P., Blain, A.W., Owen, F.N., Kerr, T.H., & Cowie, L.L. 2000, *MNRAS*, 315, 200

Ivison, R.J., Smail, I., Frayer, D.T., Kneib, J.-P., & Blain, A.W. 2001, *ApJ*, 561, L45

Ivison, R.J., et al. 2002, *MNRAS*, 337, 1

Kashikawa, N., et al. 2002, *PASJ*, 54, 819

Kneib, J.-P., Ellis, R.S., Smail, I., Couch, W.J., & Sharples, R.M. 1996 *ApJ* 471, 643

Kormann, R., Schneider, P., & Bartelmann, M. 1994, A&A, 284, 285

Landolt, A.U. 1992, AJ, 104, 340

Ledlow, M.J., Smail, I., Owen, F.N., Keel, W.C., Ivison, R.J., & Morrison, G.E. 2002, ApJ, 577, L79

Lilly, S.J., Eales, S.A., Gear, W.K.P., Hammer, F., Le Févre, O., Crampton, D., Bond, J.R., & Dunne, L. 1999, ApJ, 518, L641

Lutz, D. et al. 2001 A&A, 378, L70

Miyazaki, S., et al. 2002, PASJ, 54, 833

Moustakas, L.A., Davis, M., Graham, J.R., Silk, J., Peterson, B.A., & Yoshii, Y. 1997, ApJ, 475, 445

Motohara, K., et al. 2002, PASJ, 54, 315

Pettini, M., Steidel, C.C., Adelberger, K.L., Dickinson, M., & Giavalisco, M. 2000, ApJ, 528, 96

Prevot, M.L., Lequeux, J., Prevot, L., Maurice, E., & Rocca-Volmerange, B. 1984, A&A, 132, 389

Pozzetti, L., & Mannucci, F. 2000, MNRAS, 317, L17

Roche, N.D., Almaini, O., Dunlop, J., Ivison, R.J., & Willott, C.J. 2002, MNRAS, 337, 1282

Schneider, P., Ehlers, J., & Falco, E.E. 1992, Gravitational Lenses (Berlin:Springer) p266

Scott, S.E., et al. 2002, MNRAS, 331, 817

Shapley, A., Steidel, C.C., Adelberger, K.L., Dickinson, M., Giavalisco, M., & Pettini, M. 2001, ApJ, 562, 95

Smail, I., Ivison, R.J. & Blain, A.W. 1997, ApJ, 490, L5

Smail, I., Ivison, R.J., Blain, A.W., & Kneib, J.-P. 1998, ApJ, 507, L21

Smail, I., Ivison, R.J., Kneib, J.-P., Cowie, L.L., Blain, A.W., Barger, A.J., Owen, F.N., & Morrison, G. 1999, MNRAS, 308, 1061

Smail, I., Ivison, R.J., Blain, A.W. & Kneib, J.-P. 2002a, MNRAS, 331, 495

Smail, I., Owen, F.N., Morrison, G.E., Keel, W.C., Ivison, R.J. & Ledlow, M.J. 2002b, ApJ, 581, 844

Smith, G.P., Treu, T., Ellis, R.S., & Smail, I. 2001, ApJ, 562, 635

Smith, G.P., et al. 2002, MNRAS, 330, 1

Smith, J.A., et al. 2002, AJ, 123, 2121

Stanford S.A., Eisenhardt, P.R., & Dickinson, M. 1998, ApJ, 492, 461

Stanford S.A., Eisenhardt, P.R., Dickinson, M., Holden, B.P., & De Propris, R. 2002, ApJS, 142, 153

Steidel, C.C., Adelberger, K.L., Giavalisco, M., Dickinson, M., & Pettini, M. 1999, ApJ, 519, 1

Thompson, D., et al. 1999, ApJ, 523, 100

van Dokkum, P.G., et al. 2003, ApJ, 587, L83

Webb, T.M., et al. 2002, ApJ, 582, 6

Wehner, E.H., Barger, A.J., & Kneib, J.-P. 2002, ApJ, 577, L83

Waskett, T.J., et al. 2003, MNRAS, 341, 1217

Williams, L.L.R., Navarro, J.F., & Bartelmann, M. 1999, ApJ, 527, 535

Wu, X.P., Chiueh, T., Fang, L.-Z., & Xue, Y.-J. 1998, MNRAS, 301, 861

Yagi, M., Kashikawa, N., Sekiguchi, M., Doi, M., Yasuda, N., Shimasaku, K., & Okamura, S. 2002, AJ, 123, 66

Yun, M.S., & Carilli, C.L. 2002, ApJ, 568, 88

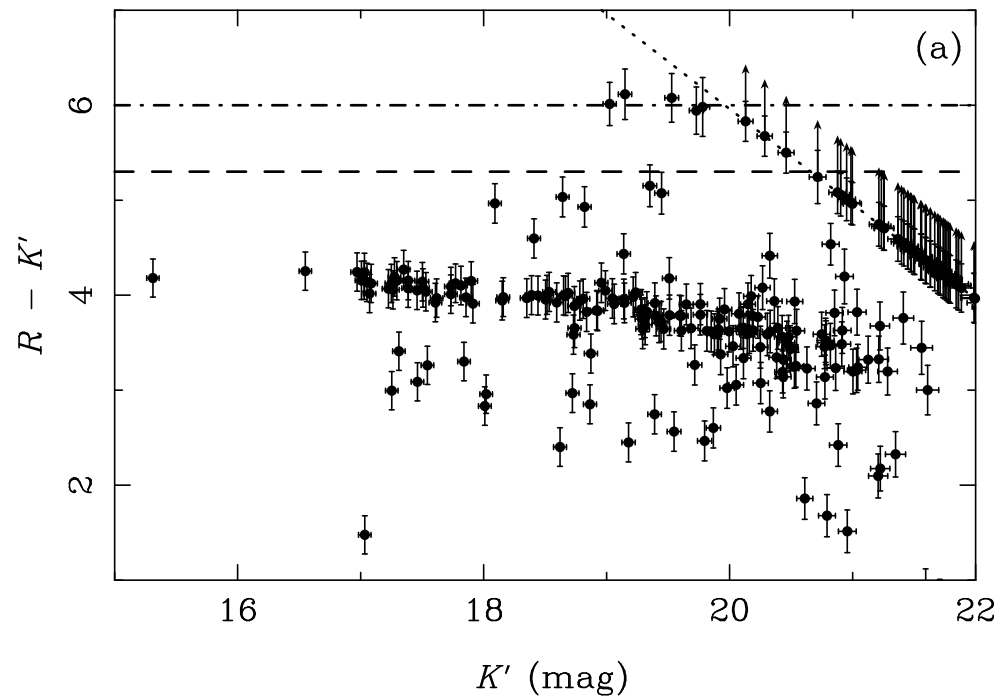
Figure Captions

- Figure 1. (a) K' vs $R_c - K'$ plot for MS 0451.6 – 0305. Color of $R_c - K' = 5.3$ and 6.0, which represent those for EROs, are shown by the dashed and dash-dotted line, respectively. The line indicating the 2σ limit of the R_c -band image is also shown. (b) Same figure for MS 0440.5 + 0204.
- Figure 2. True-color $R_c I_c K'$ image of MS 0451.6 – 0305 (using R_c and I_c data by FOCAS and a K' image by CISCO). This is a $2' \times 2'$ field of view. We identify several very red objects mainly detected in K' image.
- Figure 3. Sky distributions of EROs in the regions of (a) MS 0451.6 – 0305 and (b) MS 0440.5 + 0204. Filled red circles, filled orange stars, filled orange circles represent ERO with $R_c - K' \geq 6.0$, ones with $5.3 \leq R - K' \leq 6.0$ with and without upper limit value of R_c magnitudes, respectively. Triangles represent other sources detected in K' -band image for those fields. Regions encircled by dotted lines are showing the area we used for surface density calculations. The dashed line in (b) is showing the edge of F702W image. Central coordinates in J2000.0 for both fields are denoted at the top of the panels.
- Figure 4. K' image of the area around SMM J 04542 – 0301 with an overplotted SCUBA contour map by Chapman et al. (2002a). The contour levels represent the 2σ to 4σ detection levels. EROs around the SCUBA source are represented as “A1” to “A4” and “E”, “F”, and “G” with red rectangles, and optically bright red objects($R_c - K' \sim 5$) “B”, “C”, and “D” are also shown along with purple ones. The arc, which is clearly visible in the optical images, is denoted as “Blue Arc”.
- Figure 5. $R_c - K'$ vs $J - K'$ diagram for the objects with red colors in the MS 0451.6 – 0305 region. The dotted lines indicate the boundary between passively evolved galaxies (left side) and dusty starbursts (right side) with an extremely red color($R_c - K' = 5.3$). The objects which are identified near the extended SCUBA source are denoted as in figure 4. The curves indicate the track of elliptical galaxies(solid line) and dusty starbursts(dashed line) with a redshift range of 1 to 4 (redshifts 1.0, 2.0, 3.0 are denoted for each track). The details can be referred to in the text.
- Figure 6. FOCAS R_c and I_c band and SuprimeCam B and z' images around SMM J 04541 – 0302 in MS 0451.6 – 0305. The field sizes are 30×30 arcsec 2 . A contour map of SCUBA detection is overplotted on the R_c band image with the same levels as in figure 4.
- Figure 7. F702W and K' images around SMM J 04433 + 0210 in MS 0440.5 + 0204.

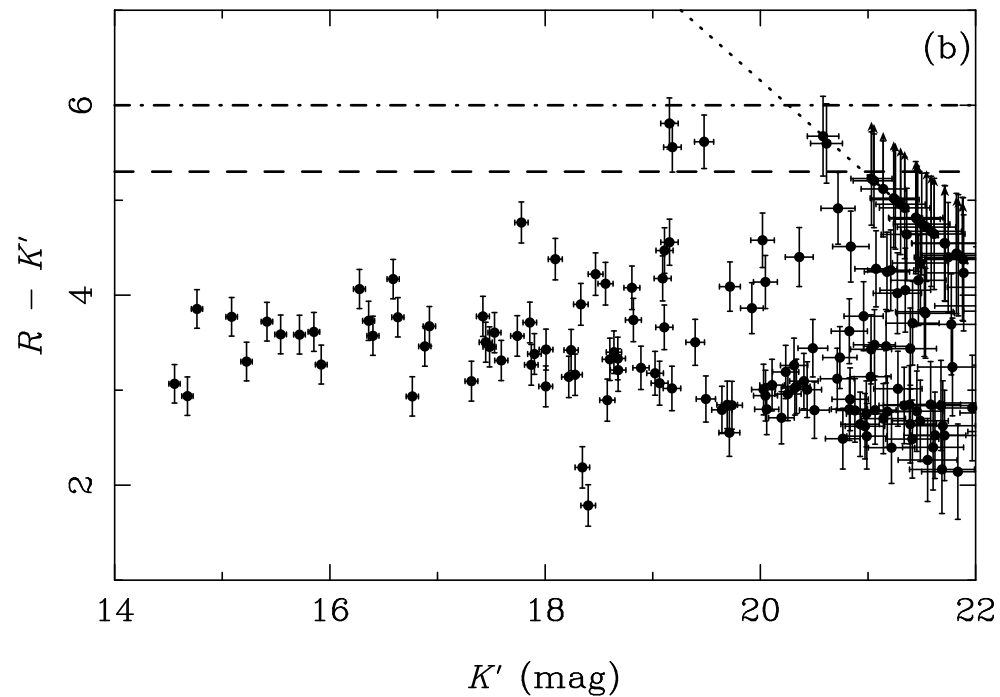
EROs are denoted as “A”, “B”, and “C”. “B” is the optical counterpart of the sub-mm source(“N4” in Frayer et al. 2003) at $z = 2.51$. Field sizes are 30×30 arcsec 2 . A bright galaxy neighboring “B” is “N1” in Smail et al. (1999). The overplotted contours in K' band image are $850 \mu\text{m}$ map in Smail et al. (1998).

- Figure 8. Cumulative area of the source plane in our survey at $z = 1.5$ that experiences magnification greater than μ .
- Figure 9. Amplification-corrected surface densities of EROs for surveyed regions. The corrections were applied assuming a single source plane at $z_{\text{source}} = 1.5$, as discussed in the text. The triangles indicate the cumulative surface densities for MS 0440.5 + 0204, the filled pentagons and circles for MS 0451.6 – 0305 within a small region as shown in figure ??, and for the whole region, respectively. The open circles show the results of G.P. Smith et al.(2002), and the open squares represent those by Wehner et al.(2002). We also plotted the results of field ERO searches by Daddi et al. (2000), Moustakas et al. (1997), and Roche et al. (2002). We plotted them without any correction for the data with $R_c - K > 5.0$ or $I - K > 4.0$. The uncertainties for our data are 1σ , based on the Poisson distribution.
- Figure 10. K' image of MS 0451.6 – 0305 with the contour of soft (0.2–1.5 keV) X-ray image taken by Chandra with a 10 ks exposure overplotted. The levels show between 1.0×10^{-8} to 5.0×10^{-8} photons cm $^{-2}$ s $^{-1}$ pix $^{-1}$ with the same interval. The critical curves for the source at $z_{\text{source}} = 1.2, 1.5, 2.0, 2.5$, and 3.0 are also shown as dotted blue, light blue, green, orange and red lines, respectively. The objects denoted in figure 4 are all shown encircled by squares (Red rectangles represent EROs.).
- Figure 11. Fitted SEDs for 6 (extremely) red objects around SMM J 04542 – 0301.

MS 0451.6–0305



MS 0440.5+0204

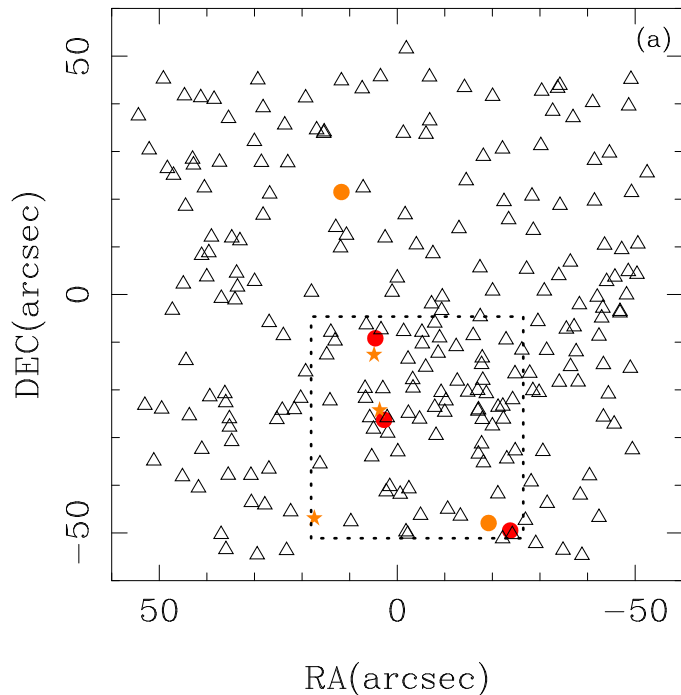


This figure "fig2.jpg" is available in "jpg" format from:

<http://arxiv.org/ps/astro-ph/0308064v1>

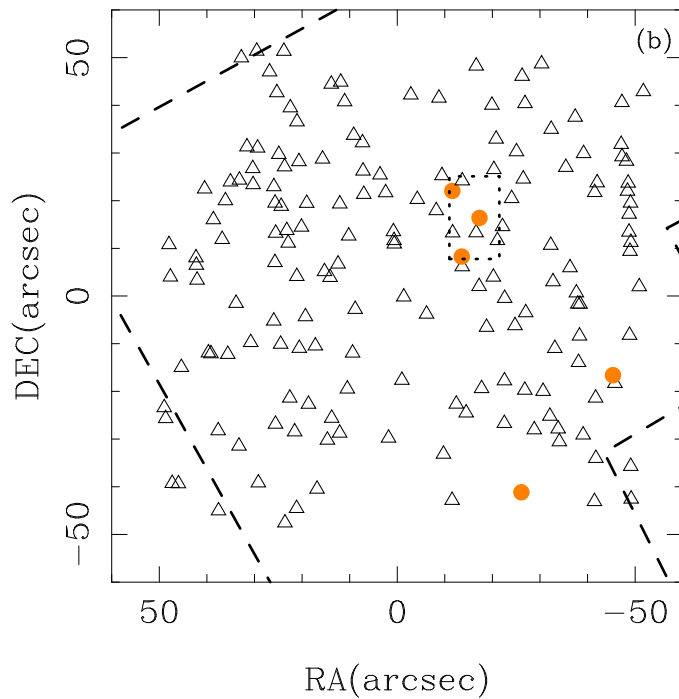
MS 0451.6-0305

(RA,DEC)=(04:54:12.5, -03:00:35.0)



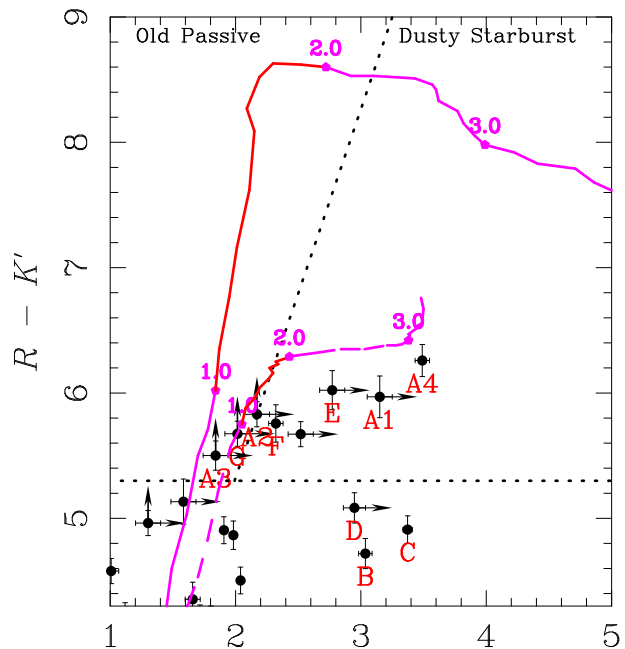
MS 0440.5+0204

(RA,DEC)=(04:43:08.4,+02:10:08.0)



This figure "fig4.jpg" is available in "jpg" format from:

<http://arxiv.org/ps/astro-ph/0308064v1>

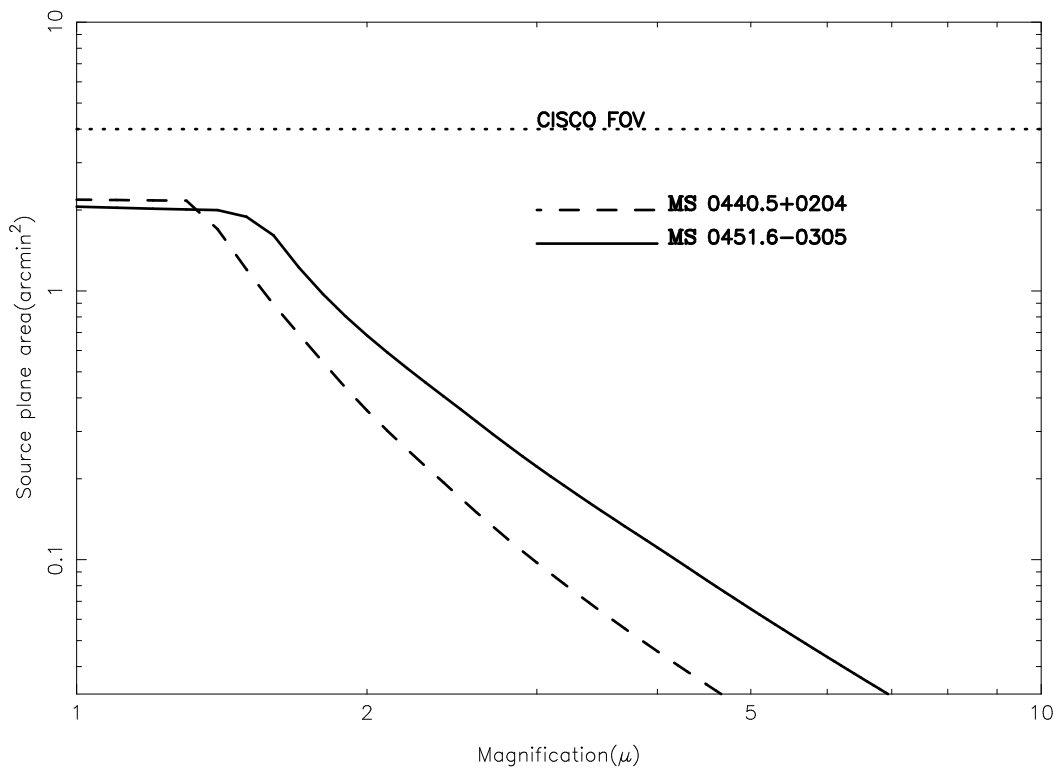
 $J - K'$

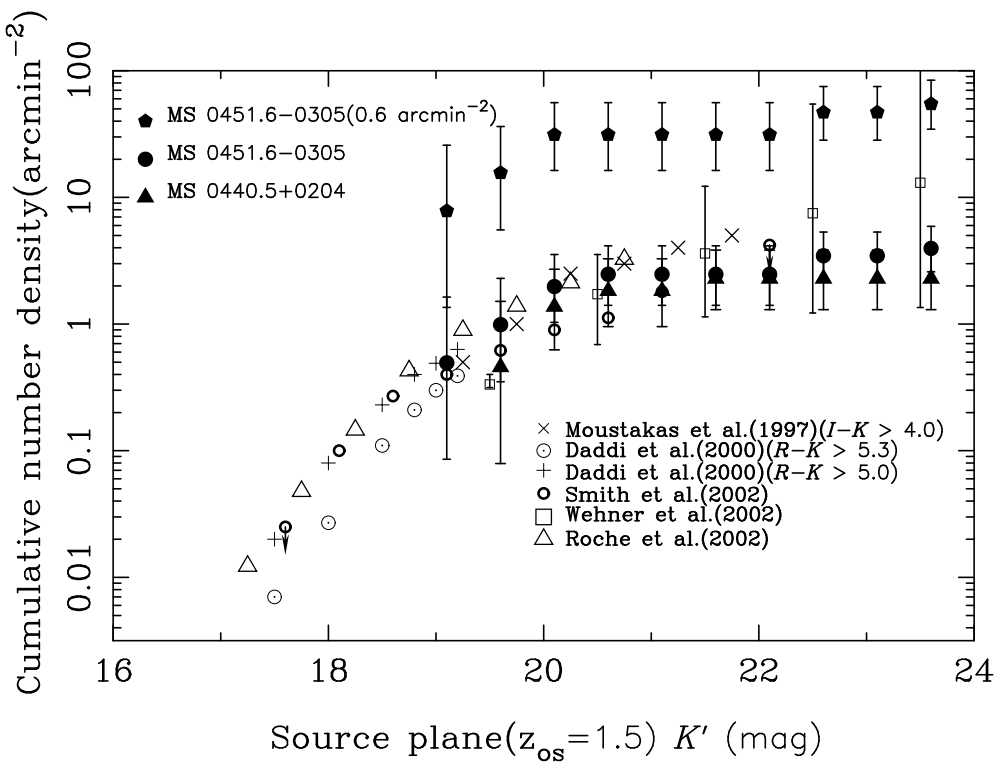
This figure "fig6.jpg" is available in "jpg" format from:

<http://arxiv.org/ps/astro-ph/0308064v1>

This figure "fig7.jpg" is available in "jpg" format from:

<http://arxiv.org/ps/astro-ph/0308064v1>





This figure "fig10.jpg" is available in "jpg" format from:

<http://arxiv.org/ps/astro-ph/0308064v1>

This figure "fig11.jpg" is available in "jpg" format from:

<http://arxiv.org/ps/astro-ph/0308064v1>